RESEARCH ARTICLE
PLANETARY SCIENCES

Earth and Planetary Physics
6: 451–464, 2022
doi: 10.26464/epp2022040

A comparison of MLT wind between meteor radar chain data and SD-WACCM results

BaoZhu Zhou[1,2], XiangHui Xue[1,2,3,4*], Wen Yi[1,2*], HaiLun Ye[1,2], Jie Zeng[1,2], JinSong Chen[5], JianFei Wu[1,2], TingDi Chen[1,2], and XianKang Dou[1,6]

[1]CAS Key Laboratory of Geospace Environment, Department of Geophysics and Planetary Sciences, University of Science and Technology of China, Hefei 230026, China;

[2]Mengcheng National Geophysical Observatory, School of Earth and Space Sciences, University of Science and Technology of China, Hefei 230026, China;

[3]Hefei National Laboratory for the Physical Sciences at the Microscale, University of Science and Technology of China, Hefei 230026, China;

[4]CAS Center for Excellence in Comparative Planetology, Hefei 230026, China;

[5]National Key Laboratory of Electromagnetic Environment, China Research Institute of Radiowave Propagation, Qingdao 266107, China;

[6]Electronic Information School, Wuhan University, Wuhan 430072, China

Key Points:

- We present the seasonal variation in and latitudinal features of the mean horizontal wind in the mesosphere and lower thermosphere (MLT) region observed by a meteor radar chain.
- We compare the wind in the MLT between meteor radar observations and a simulation obtained by the Whole Atmosphere Community Climate Model.
- A strong eastward wind in the MLT region displays a clear latitudinal change from summer to spring as the latitude decreases.

Citation: Zhou, B. Z., Xue, X. H., Yi, W., Ye, H. L., Zeng, J., Chen, J. S., Wu, J. F., Chen, T. D., and Dou, X. K. (2022). A comparison of MLT wind between meteor radar chain data and SD-WACCM results. *Earth Planet. Phys.*, *6*(5), 451–464. http://doi.org/10.26464/epp2022040

Abstract: A meteor radar chain located along the 120°E meridian in the Northern Hemisphere from low to middle latitudes provides long-term horizontal wind observations of the mesosphere and lower thermosphere (MLT) region. In this study, we report a seasonal variation and its latitudinal feature in the horizontal mean wind in the MLT region observed by six meteor radar instruments located at Mohe (53.5°N, 122.3°E), Beijing (40.3°N, 116.2°E), Mengcheng (33.4°N, 116.5°E), Wuhan (30.6°N, 114.4°E), Kunming (25.6°N, 108.3°E), and Fuke (19.5°N, 109.1°E) stations. In addition, we compare the wind in the MLT region measured by the meteor radar stations with those simulated by the Whole Atmosphere Community Climate Model (WACCM). In general, the WACCM appears to capture well the seasonal and latitudinal variations in the zonal wind component. In particular, the temporal evolution of the eastward zonal wind maximum shifts from July to May as the latitude decreases. However, the simulated WACCM meridional wind exhibits differences from the meteor radar observations.

Keywords: meteor radar chain; MLT horizontal wind; tide; SD-WACCM

1. Introduction

The mesosphere and lower thermosphere (MLT) are important regions for understanding the dynamic processes occurring between the lower atmosphere and upper atmosphere. Detailed knowledge of the horizontal winds in the MLT region is essential for studying the short-term dynamics and long-term climate of the middle and upper atmosphere. Accurate and continuous observations of the MLT regions are quite difficult. Ground-based optical instruments, such as lidars and airglow spectrometers, can provide high temporal resolution and accurate wind measurements but are limited to clear sky and often to nighttime conditions. Ground-based radio radars, such as MF (medium frequency) and VHF (very high frequency) radars, are used to measure the neutral horizontal wind in the MLT, but such radars are not widely distributed in some latitudes. Meteor radar systems have been widely employed for investigating the MLT for decades, especially for the neutral winds in the MLT region. Because of the advantage that meteor radars operate continuously under all weather conditions, their measurements are used all over the world to explor the dynamics and climate of the MLT (e.g., Dowdy et al., 2001; Hocking et al., 2004; Holdsworth et al., 2006; Reid et al., 2006; Hall et al., 2006, 2012; Kumar and Hocking, 2010; Stober et al., 2012; Lee et al., 2016; Liu LB et al., 2016, 2017; Yi W et al., 2016, 2019a, 2021; Li GZ et al., 2018; Ma Z et al., 2018; Gong Y et al., 2020; Wang JY et al., 2020; Huang YY et al., 2022).

In addition to such empirical observations by radar techniques, atmospheric models have also been used to study the mean wind.

Correspondence to: X. H. Xue, xuexh@ustc.edu.cn
W. Y, yiwen@ustc.edu.cn
Received 03 JAN 2022; Accepted 06 APR 2022.
Accepted article online 15 JUL 2022.

Model predictions have been used as the background winds for wave propagation studies and can be refined through comparison with empirical measurements. Horizontal Wind Model-07 (HWM07) provides an exquisite wind structure with which to study atmospheric dynamics (Hedin et al., 1996; Drob et al., 2008, 2015; Emmert et al., 2008). Another model, specific dynamics (SD) version 4 of the Whole Atmosphere Community Climate Model (SD-WACCM) (Lamarque et al., 2012) can also be used to study seasonal variations and long-term changes in MLT winds. Recently, Borchert et al. (2019) compared a first 15-year-long climatology run with the Upper Atmosphere ICOsahedral Non-hydrostatic (UA-ICON) with gravity wave parameterization. Stober et al. (2021) presented a climatological comparison of WACCM-X(SD), and other atmosphere models, with ground-based meteor radar observations at middle and polar latitudes in the Northern and Southern Hemisphere

In this study, we use a meteor radar chain located along the 120°E meridian in China at different latitudes to study the seasonal variations and latitudinal differences of the MLT horizontal wind. Descriptions of the instrument datasets and the method are presented in Section 2. The meteor radar wind characteristics and seasonal variations at different latitudes are presented in Section 3. Composite-year comparisons between the observations and the WACCM simulation are shown in Section 4. A discussion of the zonal wind phenomenon appears in Section 5. Finally, a summary of our results is provided.

2. Instruments and Model Data

The horizontal average wind data used in this study were collected from six meteor radars located at Mohe (53.5°N, 122.3°E), Beijing (40.3°N, 116.2°E), Mengcheng (33.4°N, 116.5°E), and Wuhan (30.6°N, 114.4°E), at midlatitudes, and Kunming (25.6°N, 108.3°E) and Fuke (19.5°N, 109.1°E) at the low latitudes (e.g., Liu LB et al., 2016, Yi W et al., 2019a, Zeng J et al., 2022). Table 1 and Figure 1 summarize the geographic locations and observational time periods of the six meteor radar stations used in this study. All the meteor radars belong to the Enhanced Meteor Detection Radar System (EMDR) series manufactured by ATRAD, similar to the Buckland Park meteor radar system described by Holdsworth et al. (2004). The resolution of the meteor radar wind data is 1 hour temporal and 2 km spatial.

In this study, we also used a specific dynamics (SD) version of the WACCM, in which winds below 50–60 km are close to NASA's Modern-Era Retrospective analysis for Research and Applications (MERRA) (Lamarque et al., 2012). The horizontal resolution is 1.9° latitude × 2.5° longitude. We performed model experiments using 144 vertical model levels (termed lev144), which have 62 vertical levels from the surface to 0.42 Pa (below ~50 km), similar to MERRA, with different vertical resolutions above 0.42 Pa — the resolution decreases from 1.9 km down to approximately 500 m in the MLT (Merkel et al., 2009; Viehl et al., 2016; Gu SY et al., 2020). To verify the performance of the wind output in the WACCM simulation, we also present a comparison of winds in the MLT obtained by the meteor radar and the WACCM simulation. The output of the WACCM was consistent with that of the meteor radar, with temporal and spatial resolutions of 1 hour and 2 km and altitudes of 80 to 100 km. The time period of the WACCM simulation in this study was the entire year of 2017.

Table 1. Geographic coordinates and observational time periods for the meteor radars used in this study.

Meteor radar	Geographic coordinates	Data used in this study
Mohe	53.5°N, 122.3°E	2012-09–2021-12
Beijing	40.3°N, 116.2°E	2012-09–2021-12
Mengcheng	33.4°N, 116.1°E	2012-09–2021-12
Wuhan	30.6°N, 114.4°E	2012-10–2021-12
Kunming	25.6°N, 108.3°E	2011-04–2021-12
Fuke	19.5°N, 109.1°E	2015-08–2021-12

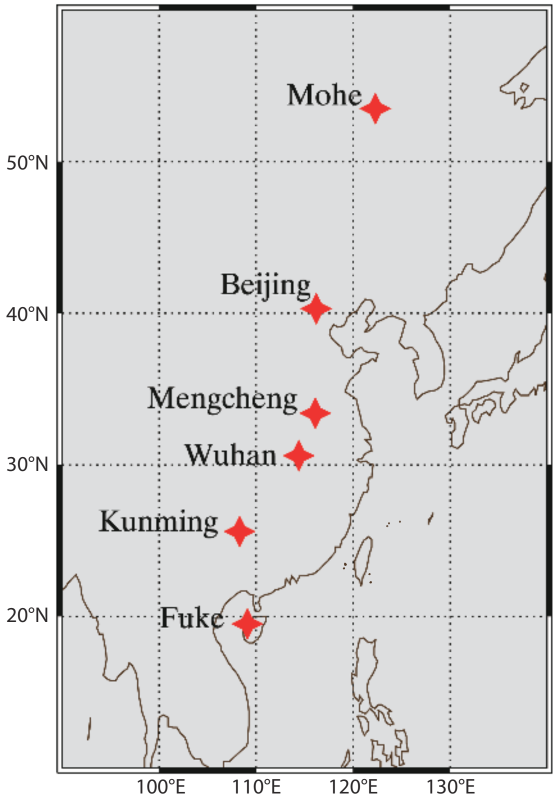

Figure 1. Locations of the six meteor radars of the meteor radar chain.

3. Seasonal Variations in the MLT Wind Observed by a Meteor Radar Chain

Figures 2 and 3 present the seasonal variations of zonal and meridional monthly mean winds observed by the six meteor radars. Figure 2 shows that the zonal winds over Mohe, Beijing, Mengcheng, and Wuhan at midlatitudes exhibit a pronounced annual oscillation (AO) (Drob et al., 2008); the Kunming and Fuke meteor radar winds, at low latitudes, mainly show semi-annual oscillations (SAO) (Vijayan and Vijayan, 1993; Dou XK et al., 2009; Venkateswara Rao et al., 2012a; Li N et al., 2015). A reversal of the mean zonal winds, from eastward to westward, occurs at about 84 to 90 km over Mohe during the summer and is also observed over Beijing, Mengcheng, and Wuhan (Ma Z et al., 2018; Jia MJ et al.,

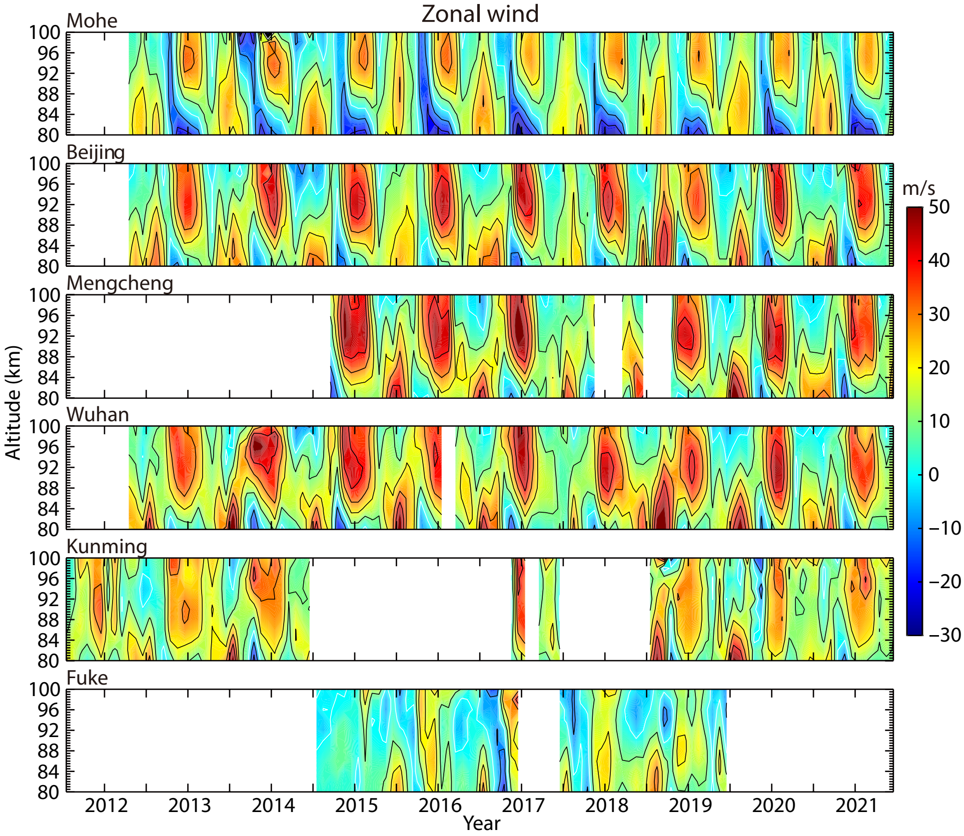

Figure 2. Variations of monthly mean zonal wind at altitudes from 80 to 100 km obtained from data collected by the Mohe, Beijing, Mengcheng, Wuhan, Kunming, and Fuke meteor radars (from top to bottom) from January 2012 to December 2021.

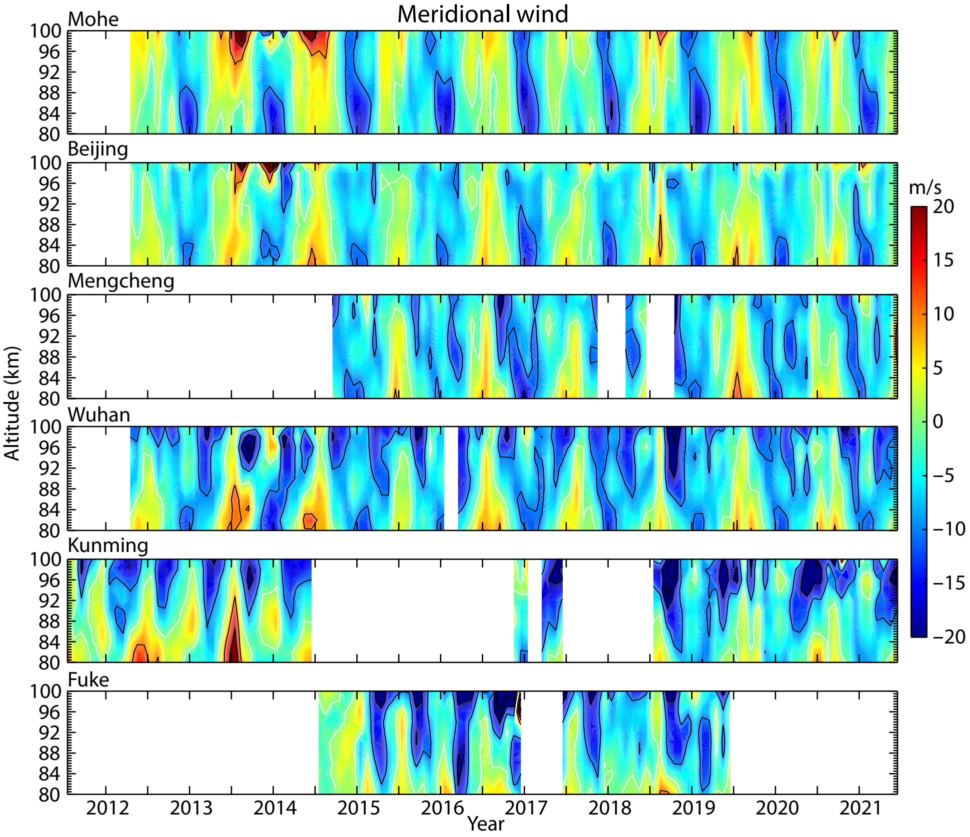

Figure 3. Same as Figures 2, but for the meridional winds.

2018). Figure 3 shows that the meridional winds over Mohe, Beijing, Mengcheng, and Wuhan exhibit primarily a pronounced annual oscillation, while the winds observed at Kunming and Fuke exhibit semi-annual oscillations. However, unlike the zonal winds, the mean meridional winds do not exhibit a summer eastward to westward reversal (as shown in Figure 3).

To further examine the periodicities present in the MLT winds data derived from the meteor radars, Lomb–Scargle (LS) periodograms are calculated for the entire observational period of the winds in each 2 km bin from 80 to 100 km. Figure 4a shows the LS spectrum of zonal wind at midlatitudes and low latitude. Generally, the AO and SAO amplitudes of the zonal wind are larger than those of the meridional wind. The periodograms of the winds over the six meteor radars show an AO and an SAO. At midlatitudes, the amplitude of the zonal wind AO is stronger than that of the SAO. The AO amplitude clearly reaches a maximum of ~25 m/s in Mengcheng, while the SAO reaches a maximum of ~12 m/s in Beijing. In Mengcheng, Wuhan, and Beijing, the zonal wind AO at 84 km has an obvious low significance level. In Beijing, the AO amplitude is much larger than that of the SAO. However, in Wuhan, the AO amplitude is similar to the SAO amplitude. Generally, the AO amplitude increases gradually as latitude decreases, while the SAO amplitude rapidly increases. At midlatitudes, the seasonal variation in the MLT wind is due predominantly to the AO.

Zonal winds also exhibit clear seasonal periodicities, with quasi-120-day and quasi-90-day oscillations. However, these seasonal periodicities are not obvious in the meridional wind. These results are comparable to those of a previous study along the 120°E longitude in NH (Yu Y et al., 2015). Referring to previous studies by Jia MJ et al. (2018), a similar result was also presented for zonal winds; they reported that an AO is evident at midlatitudes. The differences in structure observed among the six stations appear to be due mainly to their different latitudes (Jia MJ et al., 2018; Yi W et al., 2019a).

Figure 4b shows the LS spectrum of meridional wind at midlatitudes and low latitude. Both of AO and an SAO are observed clearly at Mohe, Mengcheng, Wuhan, and Fuke, whereas data from the Beijing station shows only an AO and from Kunming shows only an SAO. The AO amplitude clearly reaches a maximum

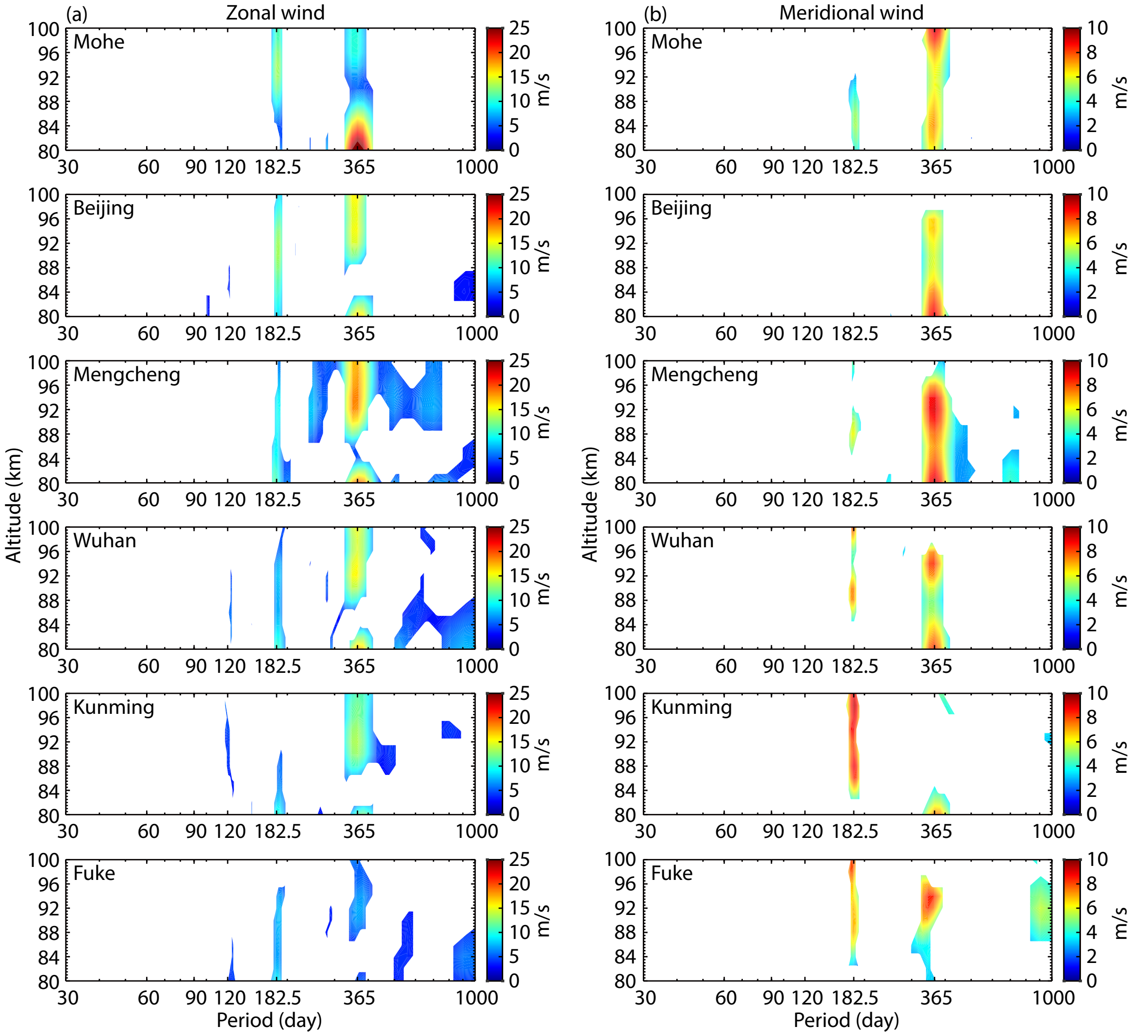

Figure 4. Contours of the Lomb–Scargle spectral relative amplitudes of the zonal winds (a) and meridional wind (b) over Mohe, Beijing, Mengcheng, Wuhan, Kunming, and Fuke stations (from top to bottom). The white areas indicate results that fell below the 95% significance level.

of ~10 m/s in Mengcheng, whereas the SAO amplitude reaches a maximum of ~8 m/s in Kunming. In Mohe, the AO amplitude is much larger than the SAO amplitude. However, in Wuhan, the AO amplitude is similar to the SAO amplitude and in Fuke, the observed AO amplitude is lower than the SAO amplitude. Thus, as latitude decreases, the AO amplitude increases slowly, while the SAO amplitude increases rapidly. This result is similar to that shown in Figure 4. The meridional wind does not exhibit clear quasi-120-day or quasi-90-day oscillations (Yi W et al., 2019b). Overall, the SAO is predominant at low latitudes, whereas the AO is obvious at midlatitudes. In both zonal and meridional winds, the AO amplitude increases slowly from Mohe to Mengcheng, as latitude decreases, while the SAO amplitude rapidly increases as latitude decreases.

Figure 5 shows the harmonic fitting results of zonal winds observed by the meteor radar chain (shown in Figure 4). From Figure 5a, it is clear that the AO in the zonal wind displays an amplitude maximum of ~20 m/s in Mengcheng. All sites have a similar trend in the AO amplitude: the AO amplitude decreases at altitudes from 100 to 94 km and from 86 to 80 km, whereas it increases at altitudes from 94 to 86 km. In Figure 5b, the SAO amplitude is much weaker than the AO amplitude. The SAO in the zonal wind displays an amplitude maximum of ~10 m/s in Beijing. The SAO amplitude shows a similar trend: the SAO amplitude increases from 100 to 96 km and from 84 to 80 km, and it decreases from 96 to 84 km. Figures 5c and 5d show the phases of the AO and SAO. In Figure 5c, the AO in the zonal wind phase shows a similar trend at altitudes from 100 to 90 km at all sites except Kunming. In Figure 5d, the SAO in the zonal wind phase shows a similar trend at altitudes from 90 to 80 km at all sites. The phases of the AO shown in Figure 5c at middle latitudes and the phases of the SAO shown in Figure 5d at low latitudes are consistent with the times the eastward and westward wind maxima occurred (as shown in Figure 2).

Figure 6 presents the harmonic fitting results of the meridional wind observed by the meteor radar chain. As shown in Figure 6a, the AO in the meridional wind exhibits an amplitude maximum of ~8 m/s in Mengcheng, which is similar to the result shown in Figure 5a. Mengcheng, Wuhan, and Beijing show the same trend: the AO amplitude decreases at altitudes from 100 to 94 km and from 86 to 80 km, whereas it increases at altitudes from 94 to 86 km. However, in Kunming and Fuke, the trend is opposite the variation at the middle latitude stations. As shown in Figure 6b, the SAO amplitude displays a maximum of ~7.5 m/s in Kunming. Similar to Figure 6b, the SAO shows the same trend at all sites: the SAO amplitude decreases at altitudes from 100 to 94 km and from 86 to 80 km, whereas it increases at altitudes from 94 to 86 km. Figures 6c and 6d show the phases of the AO and SAO. The AO in the meridional wind phase has a similar trend as that shown in Figures 5c and 5d. The phases of the AO shown in Figure 6c at

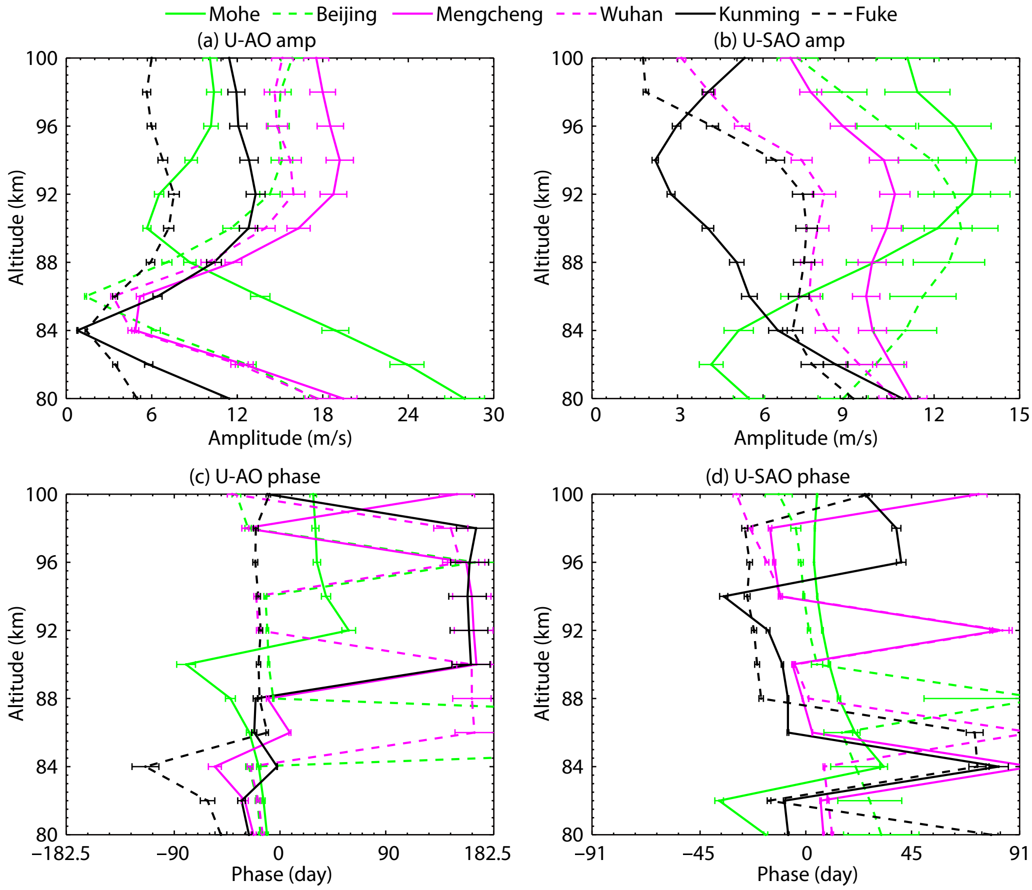

Figure 5. Harmonic fitting results for the zonal winds observed by the meteor radar chain. Amplitude (a, b) and phase (c, d) of the AO and SAO observed by all six meteor radars.

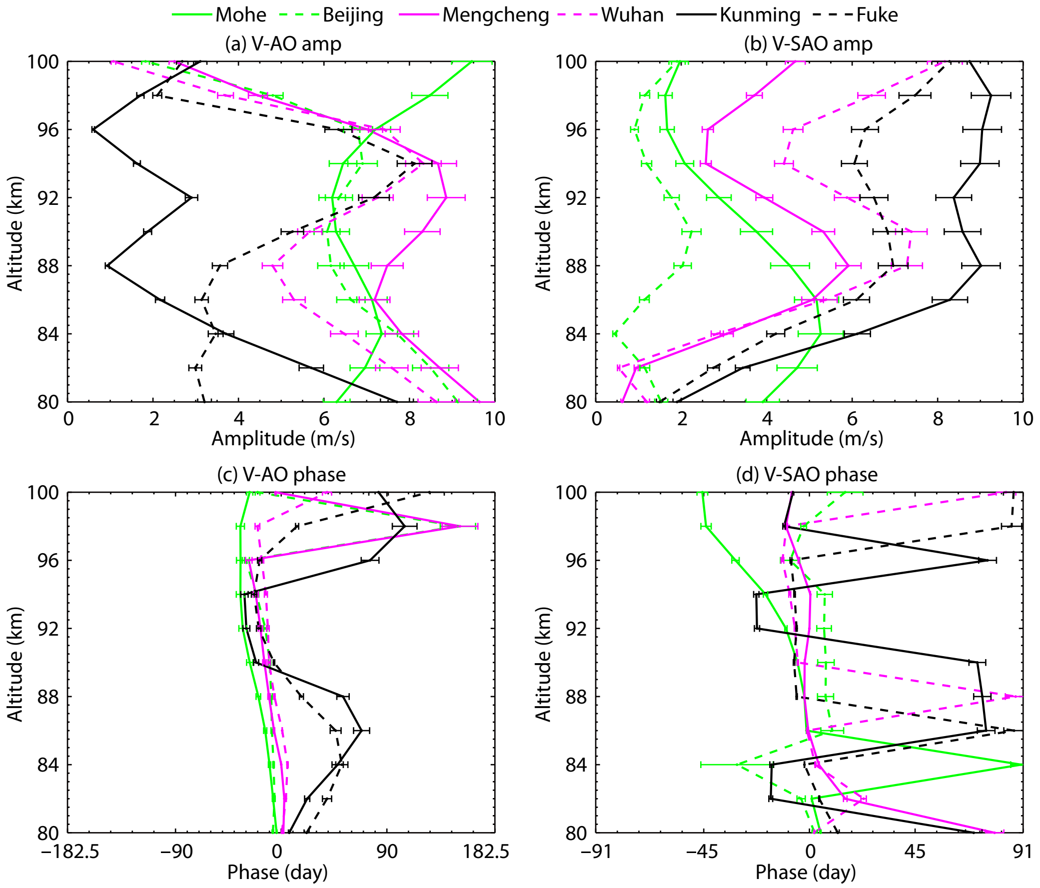

Figure 6. Same as Figure 5, but for meridional winds.

middle latitudes and the phases of the SAO shown in Figure 6d at low latitudes are consistent with the times the northward and southward wind maxima occurred (see Figure 3).

In general, the seasonal variations in wind in the MLT region are mainly associated with the AO at middle latitudes and with the SAO at low latitudes. Ma Z et al. (2018) reported a similar pattern of zonal and meridional AO wind trends in their study, and that the meridional wind SAO amplitude reached its maximum at low latitudes, which in their study was observed in data collected at Sanya (19.5°N, 105.1°E) and in this paper, at Kunming.

4. A Comparison of Wind in the MLT Obtained from the Meteor Radar Chain and the WACCM Model

Figure 7 compares the monthly mean zonal winds observed by the meteor radar array with the corresponding model results from the WACCM. The mean zonal winds observed at the six radar stations show very similar patterns. The AO can be observed between 80 and 86 km, with eastward zonal winds in autumn and winter (August to February) and westward zonal winds in summer (March to July). The AO can also be observed between 96 and 100 km, with eastward zonal winds in summer and westward zonal winds in autumn and winter. An SAO is observed between 86 and 96 km, with eastward zonal winds in winter and summer and westward zonal winds at around the Vernal equinox and the Autumn equinox. During summer, eastward zonal winds reach a peak value of 40–50 m/s at ~86 to ~90 km, decrease to zero at 86 km, and then turn westward. The reversal of the mean zonal winds from eastward to westward occurs at 90 km over Mohe and is also observed over the different latitudes of Beijing, Mengcheng, and Wuhan, which is similar to the simulation results of the WACCM, which, however, reveal only an AO over Mohe. The Mohe eastward zonal wind reaches its peak value in June and July, while the Kunming eastward zonal wind is at its maximum in May and June. As the latitude decreases, the time reversal of the zonal wind from eastward to westward also makes a transition from July to May (Jia MJ et al., 2018; Ma Z et al., 2018).

Figure 8 presents the monthly mean meridional wind observed by the meteor radar chain and a comparison with the wind in the WACCM. As shown in Figure 8, the mean meridional wind also shows a similar structure over the six meteor radar stations. With the meteor radar, the southward meridional wind peak value of ~18 m/s gradually decreases from middle latitudes to low latitudes. The AO can be observed only at the middle latitudes, with northward meridional winds in autumn and winter and southward meridional winds in summer. The SAO can be observed at low latitudes, with the northward meridional winds in spring and autumn and the southward meridional winds in summer and winter. However, the WACCM shows a different result in that the AO can be observed at middle latitudes, but with the northward meridional winds in autumn and the southward meridional winds in spring, summer, and winter. In addition, as shown in Figure 4, the

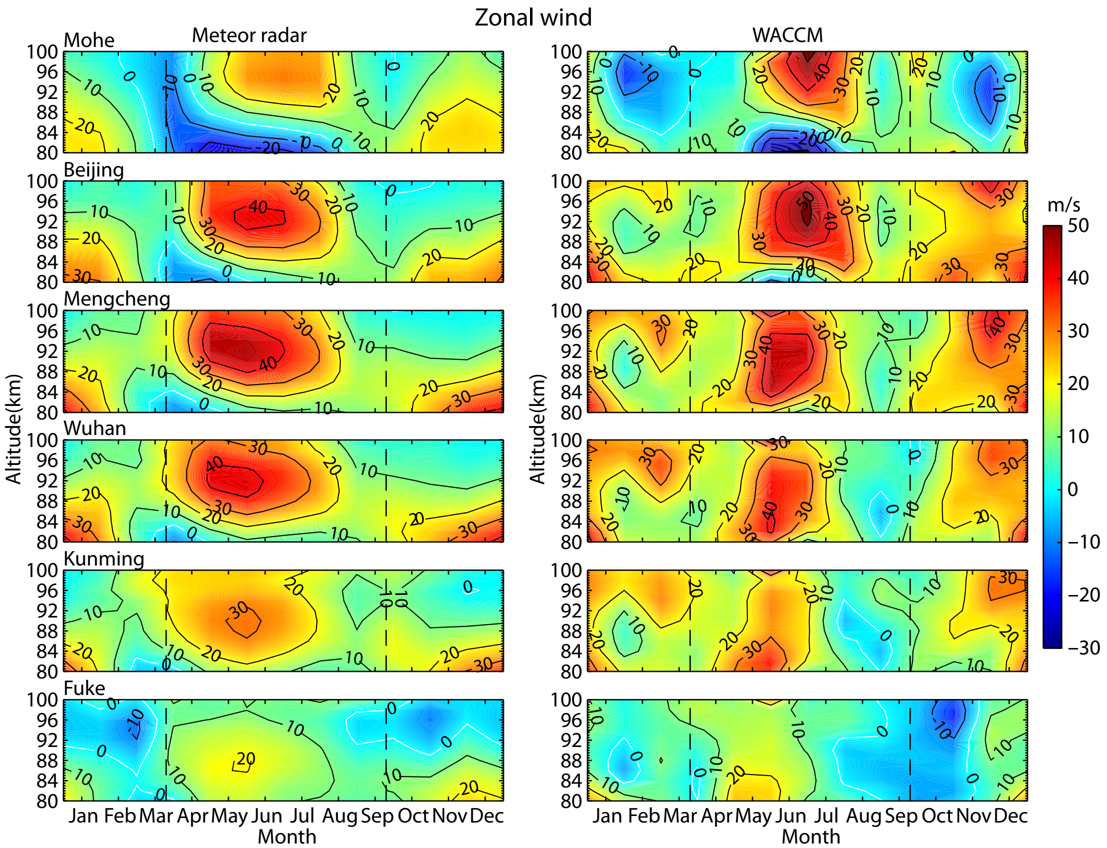

Figure 7. Comparison of monthly mean zonal wind in a composite-year obtained by meteor radar (left column) and WACCM model (right column) over Mohe, Beijing, Mengcheng, Wuhan, Kunming, and Fuke stations, respectively (from top to bottom). The vertical dashed lines indicate the spring and autumn equinoxes.

wind is mainly associated with the AO at middle latitudes and with the SAO at low latitudes. Stober et al. (2021) reported that seasonal variations in wind in the MLT observed by meteor radar have a similar structure as the WACCM.

Figure 9 compares meteor radar observations with corresponding WACCM computed winds at different altitudes. It can be seen that the WACCM zonal winds modeled for the locations of the six meteor radars exhibit trends similar to those observed by the meteor radars. The average discrepancy between modeled and meteor radar measured zonal winds is larger at 100 km and 80 km and smaller at 90 km. In comparison to zonal winds, greater differences are seen between radar measured and WACCM modeled meridional mean winds. We suggest that the WACCM can be used to study zonal winds in terms of altitude distribution but may not be suitable for studying meridional winds.

Figure 10 shows the meteor radar and WACCM zonal and meridional winds at 90 km in different months. Similar to the results shown in Figure 9, the zonal winds observed by meteor radar are in best agreement at midlatitudes with those produced by the WACCM. Moreover, the meteor radar observed meridional wind is more similar to the WACCM wind than in Figure 9. The meteor radar eastward zonal wind reaches its maximum in June and July; the westward wind reaches its maximum in May and November. The meteor radar meridional southward wind displays a maximum in February and December and the northward wind displays a maximum in September, consistent with Figures 7 and 8. The meteor radar winds are more consistent with the WACCM winds at mid-latitudes than at lower latitudes. The time of the meteor radar eastward zonal wind maximum also shifts from July to May as the latitude decreases, consistent with the results shown in Figure 7. Meanwhile, the WACCM closely reflect the characteristics of the wind observed by meteor radar in terms of the time distribution of the meridional wind. This result differs from the meteor radar winds shown in Figure 9 because the amplitude of the northward meridional wind modeled by the WACCM is too large (shown in Figure 10, right column), resulting in reversal from southward to northward of the mean meridional wind. However, the meteor radar meridional wind and the WACCM meridional wind are similar in terms of time distribution. Therefore, the WACCM can be used to study the distribution of wind with time regardless of amplitude (Stober et al., 2021).

5. Discussion

The mean wind in the MLT is substantially controlled by tides and gravity waves (GWs), carrying energy and momentum from their source regions to the altitude of their dissipation. In the analysis above, we compared the winds observed by meteor radar over a region of China with the simulation results of the WACCM. According to our comparisons, the inconsistency between the meteor radar and the WACCM means the meridional winds are

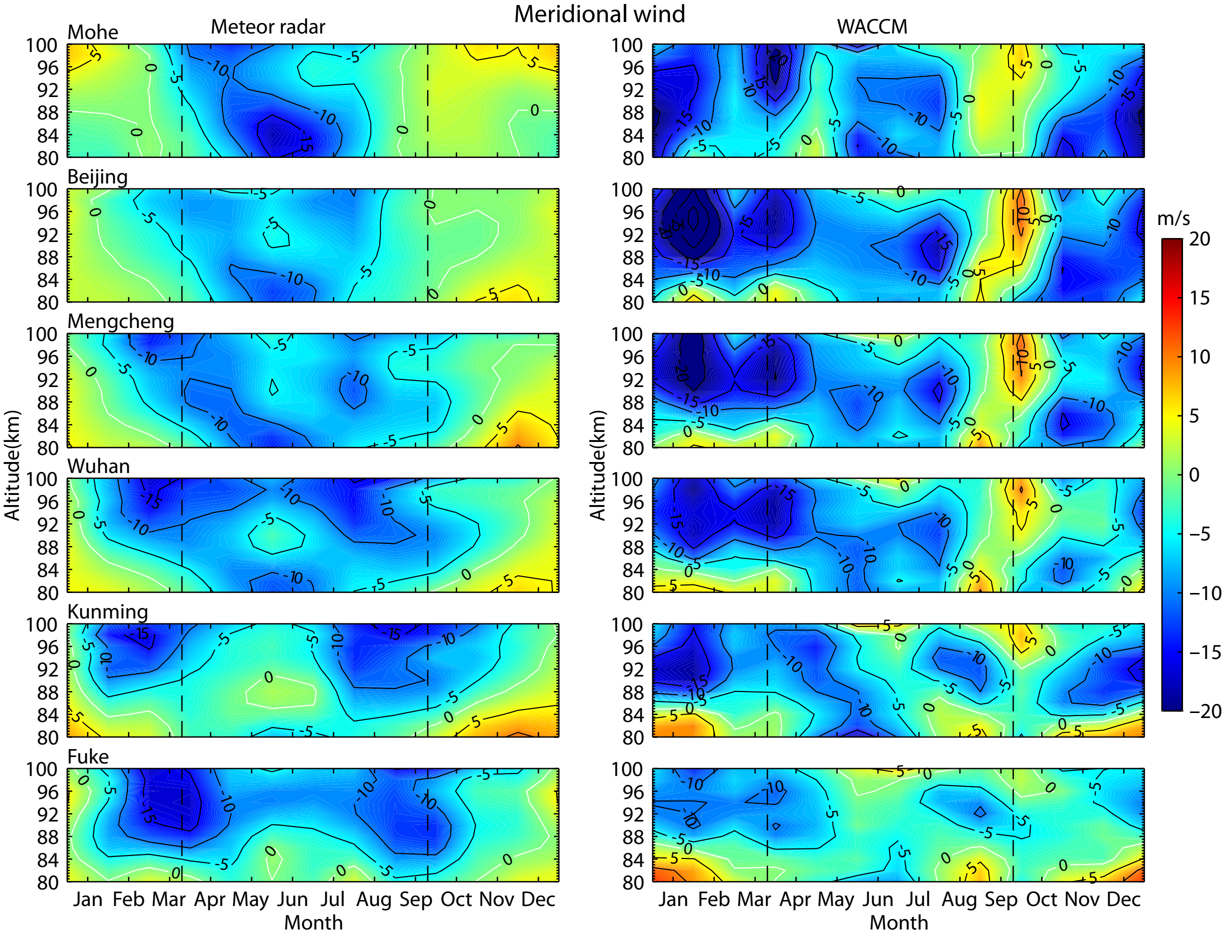

Figure 8. Same as Figure 7, but for meridional winds.

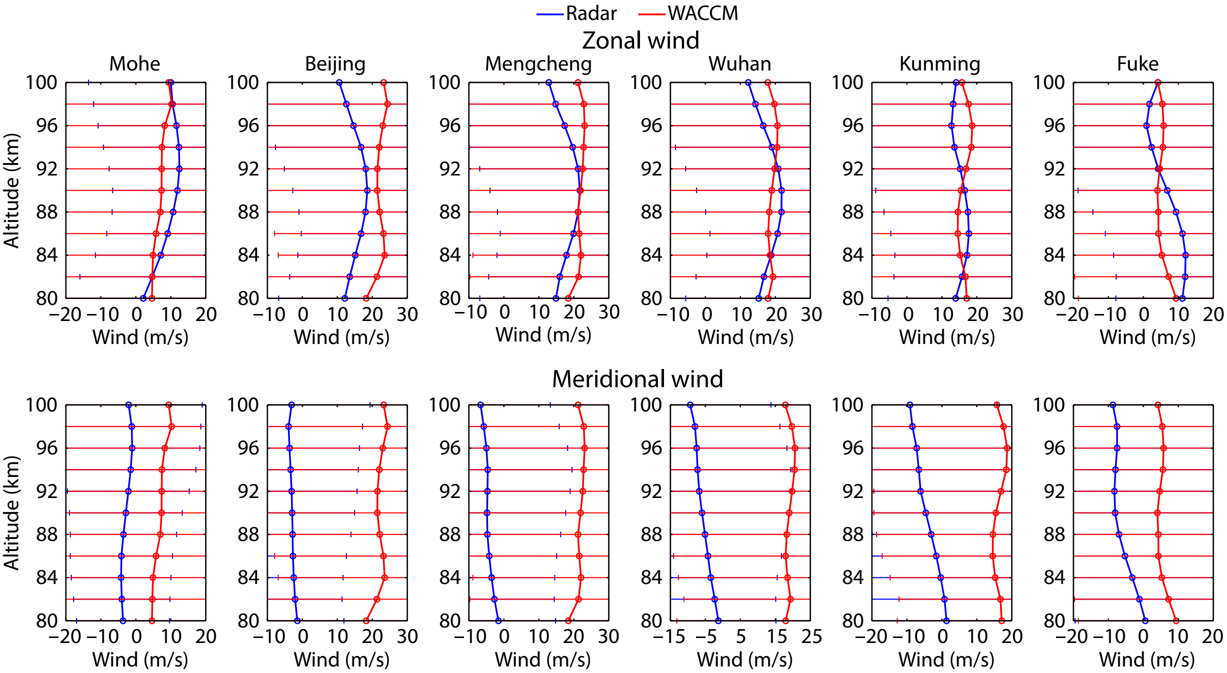

Figure 9. Vertical comparisons of the zonal (top panel) and meridional (bottom panel) mean winds at altitudes from 80 to 100 km between meteor radars and the WACCM over Mohe, Beijing, Mengcheng, Wuhan, Kunming, and Fuke (from left to right). The error bars indicate the standard deviations.

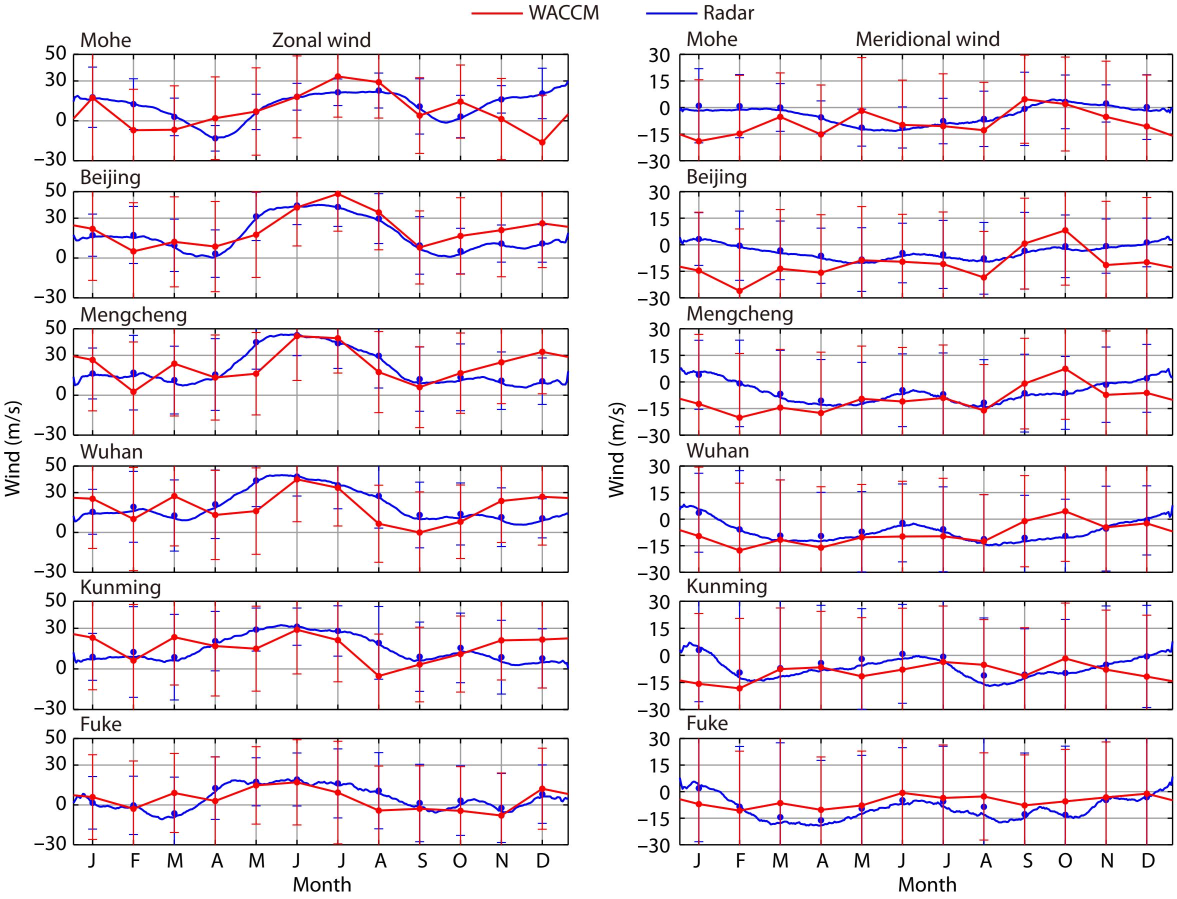

Figure 10. Temporal comparisons of the zonal (left) and meridional (right) mean winds at 90 km between meteor radars and the WACCM over Mohe, Beijing, Mengcheng, Wuhan, Kunming, and Fuke (from top to bottom). The error bars indicate the monthly standard deviations.

notably more different than that of the zonal winds, as shown in Figure 9.Therefore, we estimate the tidal component using both the meteor radar measurements and the WACCM wind simulations. The tidal parameters were estimated from the hourly data by considering a 3-day window that was shifted progressively by a day. To obtain daily amplitudes a least square cosine fit is used within the data window containing at least 48 data points (Guharay et al., 2021).

Figure 11 compares diurnal and semidiurnal tides obtained from meteor radar zonal wind observations and WACCM-modeled zonal winds. As shown in the left columns, the amplitudes of zonal wind diurnal tides observed by meteor radar reach their peak values of ~25 to 40 m/s in February and October. Those simulated with the WACCM reach their peak values of ~20 to 40 m/s in February and November and have similar seasonal variations as the diurnal tides observed by meteor radar. In the right columns, both the observations and the simulation show enhanced semidiurnal tides during the summer season, but radar-observed enhanced semidiurnal tide activity covered almost all the observed height.

Figure 12 shows diurnal and semidiurnal tides obtained by meteor radar observations and the WACCM simulation of meridional winds, respectively. As shown in the left columns, the amplitudes of diurnal tides in meridional winds observed by meteor radar reach their peak values of ~18 to 40 m/s in February, May, and October. The amplitudes of diurnal tides in the WACCM simulation of meridional wind reach their peak values of ~16 to 35 m/s in February, May, and November and have similar seasonal variations as the diurnal tides observed by meteor radar. As shown in the right columns, the amplitudes of semidiurnal tides in meridional winds observed by meteor radar reach their peak values of ~25 to 30 m/s in May and July. However, the amplitudes of semidiurnal tides in meridional winds from the WACCM simulation reach their peak values of ~25 to 35 m/s in January, June, and October, which is different from the semidiurnal tides by meteor radar. The WACCM simulation and meteor radar observations have significantly different seasonal variations in the semidiurnal tides of meridional winds. This may be one reason for the inconsistency between the mean meridional winds from meteor radar and the WACCM.

Different models have their special parameterizations, and they have differences in their vertical structures. Thus, they have different structures for wind in the MLT observed by meteor radar. Moreover, they have many structures that are similar to those of wind observed by meteor radar. In this study, we mainly show (see Figure 7) that the reversal of the zonal wind observed by the Mohe meteor radar occurred at a latitude of approximately 90 km. With decreasing latitude, the height at which the zonal wind reversal occurs decreases. For the zonal wind, the time of the east-

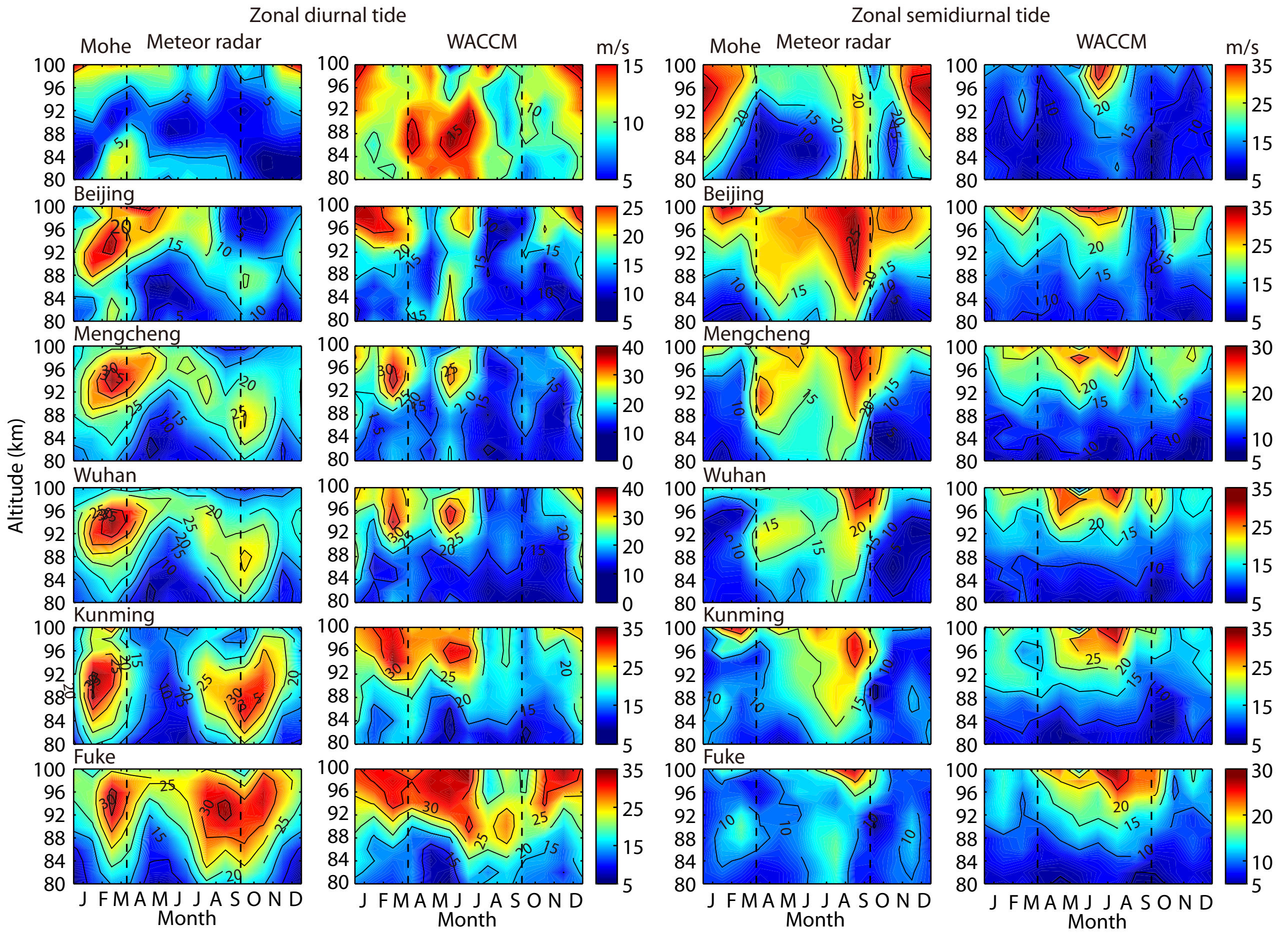

Figure 11. Diurnal tidal amplitudes obtained from zonal (U) wind measurements by the six meteor radar stations (first column on the left) and the WACCM (second column on the left). Semidiurnal tidal amplitudes obtained from zonal wind measurements by the six meteor radar stations (first column on the right) and the WACCM (second column on the right). The vertical dashed lines indicate the spring and autumn equinoxes.

ward wind maximum observed by meteor radar changes at different latitudes and slowly shifts from July to May, consistent with the results of the WACCM. In the MLT region, gravity waves not only affect the wind, but they also change the characteristics of latitudinal variation of the mesopause (Fritts, 1984; Fritts and Alexander, 2003; Jia MJ et al., 2018). Ma Z et al. (2018) reported that the wind change is mainly influenced by gravity wave forcing. Yi W et al. (2019a) reported a similar latitudinal phenomenon for the relative density of the mesopause, namely that it may be influenced by gravity wave forcing. Furthermore, many studies have shown that gravity waves are very important in the MLT (Becker and Vadas, 2018; Jia MJ et al., 2018; Sato et al., 2018). Generally, the westward gravity wave will be filtered by the westward wind in the process of upward propagation of the lower atmosphere, and the filtering effect is greater with the enhancement of the westward wind. After the filtering, a large number of eastward gravity waves will break up when they reach a certain altitude, and at the same time, they will drag the background wind field eastward. This process contributed to the wind results shown in Figure 7 (Li et al., 2012; Venkateswara Rao et al., 2012b; Day and Mitchell, 2013). It is difficult to understand how gravity waves influence zonal wind in the MLT by studying only the MLT region because meteor radar cannot provide wind measurements below 70 km.

In this study, we have shown that the winds observed by meteor radar are essentially consistent with the results of the WACCM simulation. Figure 13 shows the zonal wind in the lower atmosphere at an altitude range of 50–80 km from the simulation results of the WACCM. Figure 13 shows the zonal wind from the WACCM simulation. We can clearly see that as the latitude decreases, the maximum of the westward zonal wind at ~50 m/s obviously increases to ~60 m/s and that this happens in June. As mentioned, the westward zonal wind in the range of 50–80 km at six sites decreases with a decrease in latitude. Therefore, the breaking altitude of the eastward gravity wave also decreases. The changing altitude of the winds decreases, as shown in Figure 7. Moreover, because the breaking height of the gravity wave is reduced, the eastward zonal wind can accumulate earlier. The maximum of the eastward wind in the MLT region is generated in advance. Therefore, the time of the eastward zonal wind maximum (shown in Figure 7) is advanced as the latitude decreases. In fact, the physical mechanism cannot be comprehensively proven at the moment and thus remains an open question. Future observations and models are needed to describe and explain these phenomena more completely.

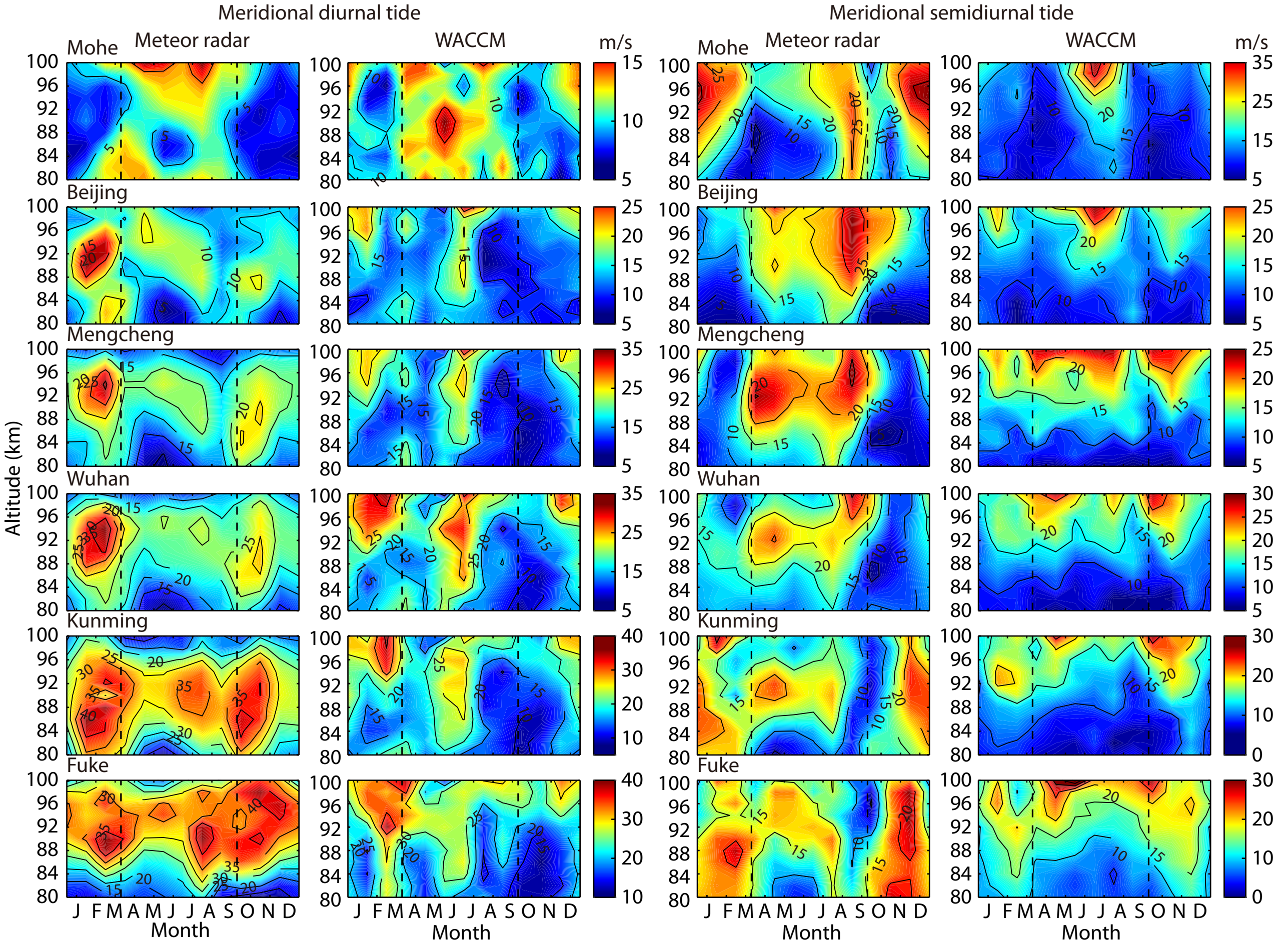

Figure 12. Same as Figure 11, but for meridional (V) winds.

6. Summary

Horizontal wind in the MLT region observed by a meteor radar chain was used to study the seasonal variations at different latitudes. The wind observations in the MLT region were carried out by six meteor radars, namely the Mohe (53.5°N, 122.3°E), Beijing (40.3°N, 116.2°E), Mengcheng (33.4°N, 116.5°E), and Wuhan (30.6°N, 114.4°E) meteor radar stations located at middle latitudes and the Kunming (25.6°N, 108.3°E) and Fuke (19.5°N, 109.1°E) meteor radar stations located at low latitudes. The wind observed by the six meteor radar stations presents obvious seasonal variations, based on comparisons with wind from the WACCM simulation. The main results can be summarized as follows:

(1) Horizontal wind in MLT region has obvious seasonal variations and latitudinal features. The SAO predominates at low latitudes, whereas the AO is obvious at middle latitudes. In both the zonal and meridional winds, the AO amplitude increases slowly from Mohe to Mengcheng as the latitude decreases, whereas the SAO amplitude increases rapidly as the latitude decreases. The reversal of the zonal wind from eastward to westward occurs at an altitude of approximately 90 km. As the latitude decreases, the altitude of the zonal wind reversal decreases. The time of the eastward zonal wind maximum observed by meteor radar occurs at different latitudes and slowly shifts from July to May, consistent with the results of the WACCM simulation.

(2) The WACCM appears to capture the seasonal and latitudinal variations in the zonal wind component well, especially the temporal evolution of the eastward zonal wind maximum, which shifts from July to May as the latitude decreases. However, the meridional wind differs between the WACCM simulation and the meteor radar observation results.

In this study, our results suggest that the reversal of the zonal wind from eastward to westward during summer may be associated with the eastward gravity wave breaking by comparison with the WACCM. Despite the differences between the meteor radar observations and model simulations, the simulated wind in the MLT region is still similar to the wind from the meteor radar observations. The present work provides a wide range of aerospace applications and has the potential to improve widely used empirical models.

Acknowledgments

This work was supported by the National Natural Science Foundation of China (Grant Nos. 42125402, 41974174, 42074181, 42188101, 41831071, 42174183, and 41904135), the B-type Strategic Priority Program of the Chinese Academy of Sciences (CAS; Grant No. XDB41000000), the Project of Stable Support for Youth Team in Basic Research Field, CAS (Grant No. YSBR-018), the Open Research Project of Large Research Infrastructures of CAS, titled

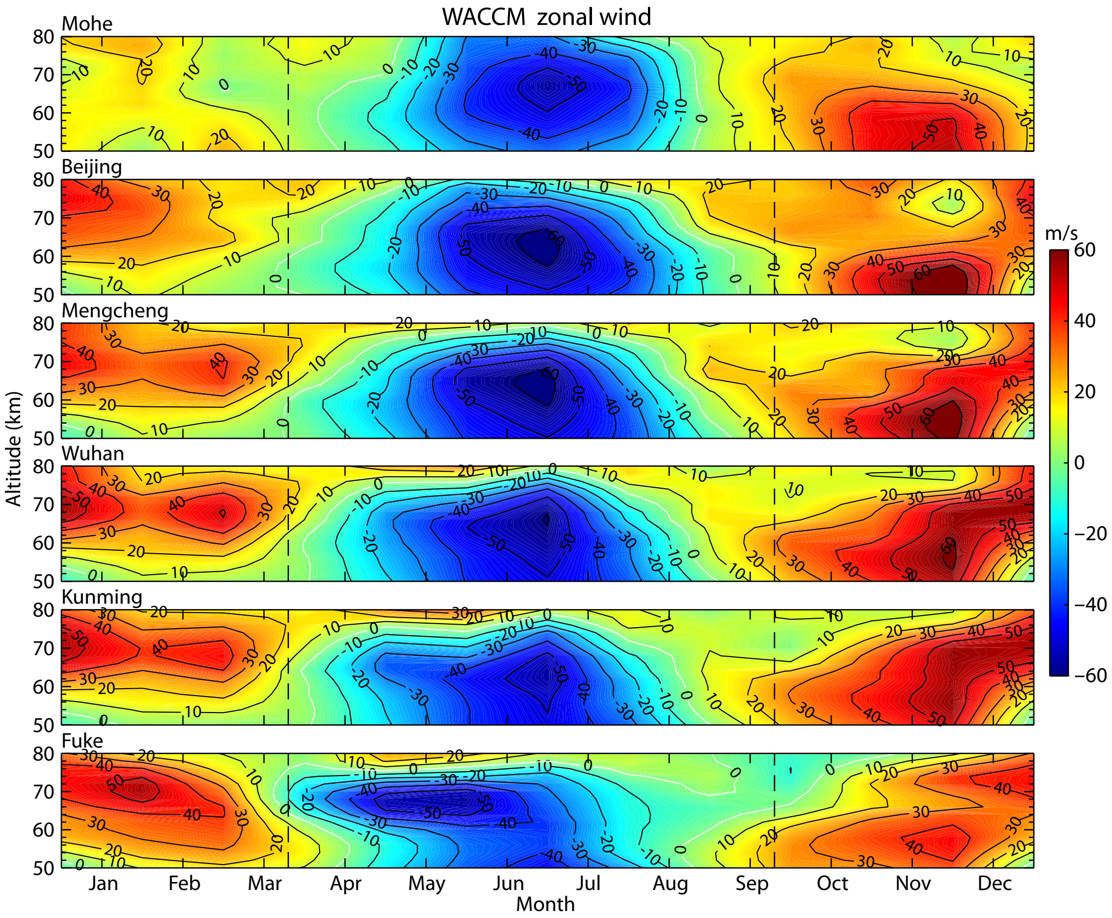

Figure 13. Monthly-mean wind in a composite-year in the zonal component of WACCM at altitudes from 50 to 80 km over Mohe, Beijing, Mengcheng, Wuhan, Kunming, and Fuke stations (top to bottom). The vertical dashed lines indicate the spring and autumn equinoxes.

"Study on the Interaction Between Low/Mid-Latitude Atmosphere and Ionosphere Based on the Chinese Meridian Project," the Fundamental Research Funds for the Central Universities (Grant No. YD3420002004), the Anhui Provincial Natural Science Foundation (Grant No. 2008085MD113), the Joint Open Fund of Mengcheng National Geophysical Observatory (MENGO-202209), and the foundation of the National Key Laboratory of Electromagnetic Environment (Grant No. JCKY2020210C614240301). We acknowledge the data storage resources from the National Space Science Data Center, National Science & Technology Infrastructure of China (http://www.nssdc.ac.cn); the provision of Mohe, Beijing, Wuhan, and Fuke meteor radar data by the Chinese Meridian Project and STERN (the Solar–Terrestrial Environment Research Network); and the provision of Kunming meteor radar data by the China Research Institute of Radiowave Propagation (CRIRP).

References

Becker, E., and Vadas, S. L. (2018). Secondary gravity waves in the winter mesosphere: Results from a high-resolution global circulation model. *J. Geophys. Res.: Atmos.*, *123*(5), 2605–2627. https://doi.org/10.1002/2017JD027460

Borchert, S., Zhou, G. D., Baldauf, M., Schmidt, H., Zängl, G., and Reinert, D. (2019). The upper-atmosphere extension of the ICON general circulation model (version: ua-icon-1.0). *Geosci. Model Dev.*, *12*(8), 3541–3569. https://doi.org/10.5194/gmd-12-3541-2019

Day, K. A., and Mitchell, N. J. (2013). Mean winds in the MLT, the SQBO and MSAO over Ascension Island (8°S, 14°W). *Atmos. Chem. Phys.*, *13*(18), 9515–9523. https://doi.org/10.5194/acp-13-9515-2013

Dou, X. K., Li, T., Xu, J. Y., Liu, H. L., Xue, X. H., Wang, S., Leblanc, T., McDermid, I. S., Hauchecorne, A., … Russell III, J. M. (2009). Seasonal oscillations of middle atmosphere temperature observed by Rayleigh lidars and their comparisons with TIMED/SABER observations. *J. Geophys. Res.: Atmos.*, *114*(D20), D20103. https://doi.org/10.1029/2008JD011654

Dowdy, A., Vincent, R. A., Igarashi, K., Murayama, Y., and Murphy, D. J. (2001). A comparison of mean winds and gravity wave activity in the northern and southern polar MLT. *Geophys. Res. Lett.*, *28*(8), 1475–1478. https://doi.org/10.1029/2000GL012576

Drob, D. P., Emmert, J. T., Crowley, G., Picone, J. M., Shepherd, G. G., Skinner, W., Hays, P., Niciejewski, R. J., Larsen, M., … Vincent, R. A. (2008). An empirical model of the Earth's horizontal wind fields: HWM07. *J. Geophys. Res.: Space Phys.*, *113*(A12), A12304. https://doi.org/10.1029/2008JA013668

Drob, D. P., Emmert, J. T., Meriwether, J. W., Makela, J. J., Doornbos, E., Conde, M., Hernandez, G., Noto, J., Zawdie, K. A., … Klenzing, J. H. (2015). An update to the Horizontal Wind Model (HWM): The quiet time thermosphere. *Earth Space Sci.*, *2*(7), 301–319. https://doi.org/10.1002/2014EA000089

Emmert, J. T., Drob, D. P., Shepherd, G. G., Hernandez, G., Jarvis, M. J., Meriwether, J. W., Niciejewski, R. J., Sipler, D. P., and Tepley, C. A. (2008). DWM07 global empirical model of upper thermospheric storm-induced disturbance winds. *J. Geophys. Res.: Space Phys.*, *113*(A11), A11319. https://doi.org/10.1029/2008JA013541

Fritts, D. C. (1984). Gravity wave saturation in the middle atmosphere: A review of theory and observations. *Rev. Geophys.*, *22*(3), 275–308. https://doi.org/

10.https://doi.org/10.1029/RG022i003p002751029/RG022i003p00275

Fritts, D. C., and Alexander, M. J. (2003). Gravity wave dynamics and effects in the middle atmosphere. *Rev. Geophys.*, *41*(1), 1003. https://doi.org/10.https://doi.org/10.1029/2001RG0001061029/2001RG000106

Gong, Y., Ma, Z., Li, C., Lv, X. D., Zhang, S. D., Zhou, Q. H., Huang, C. M., Huang, K. M., Yu, Y., and Li, G. Z. (2020). Characteristics of the quasi-16-day wave in the mesosphere and lower thermosphere region as revealed by meteor radar, Aura satellite, and MERRA2 reanalysis data from 2008 to 2017. *Earth Planet. Phys.*, *4*(3), 274–284. https://doi.org/10.26464/epp2020033

Gu, S. Y., Hou, X., Qi, J. H., TengChen K. M., and Dou, X. K. (2020). Reponses of middle atmospheric circulation to the 2009 major sudden stratospheric warming. *Earth Planet. Phys.*, *4*(5), 472–478. https://doi.org/10.26464/epp2020046

Guharay, A., Batista, P. P., and Buriti, R. A. (2021). Observations of a quasi-90-day oscillation in the MLT winds and tides over an equatorial station using meteor radar winds. *Adv. Space Res.*, *67*(10), 3125–3133. https://doi.org/10.1016/j.asr.2021.02.004

Hall, C. M., Aso, T., Tsutsumi, M., Höffner, J., Sigernes, F., and Holdsworth, D. A. (2006). Neutral air temperatures at 90 km and 70°N and 78°N. *J. Geophys. Res.: Atmos.*, *111*(D14), D14105. https://doi.org/10.1029/2005JD006794

Hall, C. M., Dyrland, M. E., Tsutsumi, M., and Mulligan, F. J. (2012). Temperature trends at 90 km over Svalbard, Norway (78°N l6°E), seen in one decade of meteor radar observations. *J. Geophys. Res.: Atmos.*, *117*(D8), D08104. https://doi.org/10.1029/2011JD017028

Hedin, A. E., Fleming, E. L., Manson, A. H., Schmidlin, F. J., Avery, S. K., Clark, R. R., Franke, S. J., Fraser, G. J., Tsuda, T., … Vincent, R. A. (1996). Empirical wind model for the upper, middle and lower atmosphere. *J. Atmos. Terr. Phys.*, *58*(13), 1421–1447. https://doi.org/10.1016/0021-9169(95)00122-0

Hocking, W. K., Singer, W., Bremer, J., Mitchell, N. J., Batista, P., Clemesha, B., and Donner, M. (2004). Meteor radar temperatures at multiple sites derived with SKiYMET radars and compared to OH, rocket and lidar measurements. *J. Atmos. Sol.-Terr. Phys.*, *66*(6-9), 585–593. https://doi.org/10.1016/j.jastp.2004.01.011

Holdsworth, D. A., Reid, I. M., and Cervera, M. A. (2004). Buckland Park all-sky interferometric meteor radar. *Radio Sci.*, *39*(5), RS5009. https://doi.org/10.1029/2003RS003014

Holdsworth, D. A., Morris, R. J., Murphy, D. J., Reid, I. M., Burns, G. B., and French, W. J. R. (2006). Antarctic mesospheric temperature estimation using the Davis mesosphere-stratosphere-troposphere radar. *J. Geophys. Res.*, *111*(D5), D05108. https://doi.org/10.1029/2005JD006589

Huang, Y. Y., Cui, J., Li, H. J., and Li, C. Y. (2022). Inter-annual variations of 6.5-day planetary waves and their relations with QBO. *Earth Planet. Phys.*, *6*(2), 135–148. https://doi.org/10.26464/epp2022005

Jia, M. J., Xue, X. H., Gu, S. Y., Chen, T. D., Ning, B. Q., Wu, J. F., Zeng, X. Y., and Dou, X. K. (2018). Multiyear observations of gravity wave momentum fluxes in the midlatitude mesosphere and lower thermosphere region by meteor radar. *J. Geophys. Res.: Space Phys.*, *123*(7), 5684–5703. https://doi.org/10.1029/2018JA025285

Kumar, G. K., and Hocking, W. K. (2010). Climatology of northern polar latitude MLT dynamics: Mean winds and tides. *Ann. Geophys.*, *28*(10), 1859–1876. https://doi.org/10.5194/angeo-28-1859-2010

Lamarque, J. F., Emmons, L. K., Hess, P. G., Kinnison, D. E., Tilmes, S., Vitt, F., Heald, C. L., Holland, E. A., Lauritzen, P. H., … Tyndall, G. K. (2012). CAM-chem: description and evaluation of interactive atmospheric chemistry in the Community Earth System Model. *Geosci. Model Dev.*, *5*(2), 369–411. https://doi.org/10.5194/gmd-5-369-2012

Lee, C., Kim, J. H., Jee, G., Lee, W., Song, I. S., and Kim, Y. H. (2016). New method of estimating temperatures near the mesopause region using meteor radar observations. *Geophys. Res. Lett.*, *43*(20), 10580–10585. https://doi.org/10.1002/2016GL071082

Li, G. Z., Ning, B. Q., Hu, L. H., Chu, Y. H., Reid, I. M., and Dolman, B. K. (2012). A comparison of lower thermospheric winds derived from range spread and specular meteor trail echoes. *J. Geophys. Res.: Space Phys.*, *117*(A3), A03310. https://doi.org/10.1029/2011JA016847

Li, G. Z., Ning, B. Q., Li, A., Yang, S. P., Zhao, X. K., Zhao, B. Q., and Wan, W. X. (2018). First results of optical meteor and meteor trail irregularity from simultaneous Sanya radar and video observations. *Earth Planet. Phys.*, *2*, 15–21. https://doi.org/10.26464/epp2018002

Li, N., Chen, J. S., Ding, Z. H., and Zhao, Z. W. (2015). Mean winds observed by the Kunming MF radar in 2008-2010. *J. Atmos. Sol.-Terr. Phys.*, *122*, 58–65. https://doi.org/10.1016/j.jastp.2014.10.011

Li, T., Liu, A. Z., Lu, X., Li, Z. H., Franke, S. J., Swenson, G. R., and Dou, X. K. (2012). Meteor-radar observed mesospheric semi-annual oscillation (SAO) and quasi-biennial oscillation (QBO) over Maui, Hawaii. *J. Geophys. Res.: Atmos.*, *117*(D5), D05130. https://doi.org/10.1029/2011JD016123

Liu, L. B., Liu, H. X., Chen, Y. D., Le, H. J., Sun, Y. Y., Ning, B. Q., Hu, L. H., and Wan, W. X. (2016). Variations of the meteor echo heights at Beijing and Mohe, China. *J. Geophys. Res.: Space Phys.*, *122*(1), 1117–1127. https://doi.org/10.1002/2016JA023448

Liu, L. B., Liu. H. X., Le, H. J., Chen, Y. D., Sun, Y. Y., Ning, B. Q., Hu, L. H., Wan, W. X., Li, N., and Xiong, J. G. (2017). Mesospheric temperatures estimated from the meteor radar observations at Mohe, China. *J. Geophys. Res.: Space Phys.*, *122*(2), 2249–2259. https://doi.org/10.1002/2016JA023776

Ma, Z., Gong, Y., Zhang, S. D., Zhou, Q. H., Huang, C. M., Huang, K. M., Dong, W. J., Li, G. Z., and Ning, B. Q. (2018). Study of mean wind variations and gravity wave forcing via a meteor radar chain and comparison with HWM-07 results. *J. Geophys. Res.: Atmos.*, *123*(17), 9488–9501. https://doi.org/10.1029/2018JD028799

Merkel, A. W., Marsh, D. R., Gettelman, A., and Jensen, E. J. (2009). On the relationship of polar mesospheric cloud ice water content, particle radius and mesospheric temperature and its use in multi-dimensional models. *Atmos. Chem. Phys.*, *9*(22), 8889–8901. https://doi.org/10.5194/acp-9-8889-2009

Reddy, C. A., and Vijayan, L. (1993). Annual and semiannual oscillations in the equatorial middle atmospheric winds. *Adv. Space Res.*, *13*(1), 373–376. https://doi.org/10.1016/0273-1177(93)90039-E

Reid, I. M., Holdsworth, D. A., Morris, R. J., Murphy, D. J., and Vincent, R. A. (2006). Meteor observations using the Davis mesosphere-stratosphere-troposphere radar. *J. Geophys. Res.: Space Phys.*, *111*(A5), A05305. https://doi.org/10.1029/2005JA011443

Sato, K., Yasui, R., and Miyoshi, Y. (2018). The momentum budget in the stratosphere, mesosphere, and lower thermosphere. *Part I: Contributions of different wave types and in situ generation of Rossby waves. J. Atmos. Sci.*, *75*(10), 3613–3633. https://doi.org/10.1175/JAS-D-17-0336.1

Stober, G., Jacobi, C., Matthias, V., Hoffmann, P., and Gerding, M. (2012). Neutral air density variations during strong planetary wave activity in the mesopause region derived from meteor radar observations. *J. Atmos. Sol.-Terr. Phys.*, *74*, 55–63. https://doi.org/10.1016/j.jastp.2011.10.007

Stober, G., Kuchar, A., Pokhotelov, D., Liu, H. X., Liu, H. L., Schmidt, H., Jacobi, C., Baumgarten, K., Brown, P., … Mitchell, N. (2021). Interhemispheric differences of mesosphere–lower thermosphere winds and tides investigated from three whole-atmosphere models and meteor radar observations. *Atmos. Chem. Phys.*, *21*(18), 13855–13902. https://doi.org/10.5194/acp-21-13855-2021

Venkateswara Rao, N., Tsuda, T., and Kawatani, Y. (2012a). A remarkable correlation between short period gravity waves and semiannual oscillation of the zonal wind in the equatorial mesopause region. *Ann. Geophys.*, *30*(4), 703–710. https://doi.org/10.5194/angeo-30-703-2012

Venkateswara Rao, N., Tsuda, T., Riggin, D. M., Gurubaran, S., Reid, I. M., and Vincent, R. A. (2012b). Long-term variability of mean winds in the mesosphere and lower thermosphere at low latitudes. *J. Geophys. Res.: Space Phys.*, *117*(A10), A10312. https://doi.org/10.1029/2012JA017850

Viehl, T. P., Plane, J. M. C., Feng, W., and Höffner, J. (2016). The photolysis of FeOH and its effect on the bottomside of the mesospheric Fe layer. *Geophys. Res. Lett.*, *43*(3), 1373–1381. https://doi.org/10.1002/2015GL067241

Yi, W., Xue, X. H., Chen, J. S., Dou, X. K., Chen, T. D., and Li, N. (2016). Estimation of mesopause temperatures at low latitudes using the Kunming meteor radar. *Radio Sci.*, *51*(3), 130–141. https://doi.org/10.1002/2015RS005722

Yi, W., Xue, X. H., Reid, I. M., Murphy, D. J., Hall, C. M., Tsutsumi, M., Ning, B. Q., Li, G. Z., Vincent, R. A., … Dou, X. K. (2019a). Climatology of the mesopause relative density using a global distribution of meteor radars. *Atmos. Chem.*

Phys., *19*(11), 7567–7581. https://doi.org/10.5194/acp-19-7567-2019

Yi, W., Xue, X. H., Chen, J. S., Chen, T. D., and Li, N. (2019b). Quasi-90-day oscillation observed in the MLT region at low latitudes from the Kunming meteor radar and SABER. *Earth Planet. Phys.*, *3*(2), 136–146. https://doi.org/10.26464/epp2019013

Yi, W., Xue, X. H., Reid, I. M., Murphy, D. J., Hall, C. M., Tsutsumi, M., Ning, B. Q., Li, G. Z., Yang, G. T., … Dou, X. K. (2021). Climatology of interhemispheric mesopause temperatures using the high-latitude and middle-latitude meteor radars. *J. Geophys. Res.: Atmos.*, *126*(6), e2020JD034301. https://doi.org/10.1029/2020JD034301

Yu, Y., Wan, W. X., Ren, Z. P., Xiong, B., Zhang, Y., Hu, L. H., Ning, B. Q., and Liu, L. B. (2015). Seasonal variations of MLT tides revealed by a meteor radar chain based on Hough mode decomposition. *J. Geophys. Res.: Space Phys.*, *120*(8), 7030–7048. https://doi.org/10.1002/2015JA021276

Wang, J. Y., Yi, W., Chen, T. D., and Xue, X. H. (2020). Quasi-6-day waves in the mesosphere and lower thermosphere region and their possible coupling with the QBO and solar 27-day rotation. *Earth Planet. Phys.*, *4*(3), 1–11. https://doi.org/10.26464/epp2020024

Zeng, J., Yi, W., Xue, X., Reid, I., Hao, X., Li, N., Chen, J., Chen, T., and Dou, X. (2022). Comparison between the Mesospheric Winds Observed by Two Collocated Meteor Radars at Low Latitudes. *Remote Sens.*, *14*, 2354. https://doi.org/10.3390/rs14102354